3D Microstructure of Tendon Collagen Fibrils using Serial Block-Face SEM and a Mechanical Model for Load Transfer

Babak N. Safa[1,2], John M. Peloquin[1], Jessica R. Natriello[1],

Jeffrey L. Caplan[3,4], and Dawn M. Elliott[1]*

[1]Department of Biomedical Engineering, University of Delaware, Newark, DE, United States

[2]Department of Mechanical Engineering, University of Delaware, Newark, DE, United States

[3]Department of Plant and Soil Sciences, University of Delaware, Newark, DE, United States

[4]Delaware Biotechnology Institute, University of Delaware, Newark, DE, United States

***Corresponding author:**
Dawn M. Elliott
University of Delaware
161 Colburn Lab,
150 Academy Street,
Newark, DE 19716
(delliott@udel.edu, T(302)-831-1295)

(Word count: ~3900)

Abstract

Tendon's hierarchical structure allows for load transfer between its fibrillar elements at multiple length scales. Tendon microstructure is particularly important, because it includes the cells and their surrounding collagen fibrils, where mechanical interactions can have potentially important physiological and pathological contributions. However, the three-dimensional microstructure and the mechanisms of load transfer in that length scale are not known. It has been postulated that interfibrillar matrix shear or direct load transfer via the fusion/branching of small fibrils are responsible for load transfer, but the significance of these mechanisms is still unclear. Alternatively, the helical fibrils that occur at the microstructural scale in tendon may also mediate load transfer, however, these structures are not well studied due to the lack of a three-dimensional visualization of tendon microstructure. In this study, we used serial block-face scanning electron microscopy (SBF-SEM) to investigate the three-dimensional microstructure of fibrils in rat tail tendon. We found that tendon fibrils have a complex architecture with many helically wrapped fibrils. We studied the mechanical implications of these helical structures using finite element modeling and found that frictional contact between helical fibrils can induce load transfer even in the absence of matrix bonding or fibril fusion/branching. This study is significant in that it provides a three-dimensional view of the tendon microstructure and suggests friction between helically wrapped fibrils as a mechanism for load transfer, which is an important aspect of tendon biomechanics. [Word count 232/250]

Keywords: SBF-SEM, Collagen fibril, Tendon, Friction, Stress mechanics

Introduction

60 Tendon's hierarchical structure allows for load transfer between its fibrillar elements across multiple length scales (Kastelic, Galeski and Baer, 1978; Screen *et al.*, 2005; Pensalfini *et al.*, 2014), which results in remarkable capabilities to withstand stress and endure repetitive loading (Snedeker and Foolen, 2017). The microscale structure and function are particularly important, because this is the
65 scale where the cells and their surrounding collagen fibrils interface, and these mechanical interactions can have important physiological and pathological contributions. However, the underlying mechanisms of load transfer between tendon fibrils are still unknown. Tendon fibrils are collagenous structures (diameter ~100 nm) that are the building blocks of tendon microstructure
70 (Kannus, 2000). The fibrils are responsible for supporting external mechanical loading. Interfibrillar matrix molecules such as glycosaminoglycan chains (GAG) have been postulated to be responsible for load transfer between fibrils (Redaelli *et al.*, 2003; Ahmadzadeh *et al.*, 2013); however, removal of a wide range of extracellular matrix components, including GAG, does not affect the mechanical
75 response (Szczesny *et al.*, 2017), or has minimal consequences (Fessel and Snedeker, 2009). It is not likely that the load transfer in tendon is solely, or majorly, mediated via interfibrillar matrix. Thus, the microscale architecture of the collagen fibrous network itself is likely to have a role in mediating load transfer.

80 Serial block-face scanning electron microscopy (SBF-SEM) makes it possible to visualize the 3D microscale architecture of tissue in great detail, and to reveal the fibrillar architecture with several mechanical implications (Starborg *et al.*, 2013; Pingel *et al.*, 2014). SBF-SEM is an advanced electron microscopy technique that takes sequential SEM images of the cross-section of tissue; these
85 images combine to provide a three-dimensional view of the microstructure (Starborg *et al.*, 2013; Hashimoto *et al.*, 2016). Using SBF-SEM with a short scan depth (8.7 μm), our group showed that there is a small fibril angular dispersion and that the fusion/branching of small fibrils might be responsible for interfibrillar load transfer (Szczesny, Edelstein and Elliott, 2014; Szczesny *et al.*,
90 2017). Longer scan depths (~100 μm) showed that fibril fusion/branching and fibril ends also exist in tendons (Svensson *et al.*, 2017), and that helical fibril patterns form during tendon development in juvenile tail tendons (Kalson *et al.*, 2015; Starborg and Kadler, 2015). The existence of helical fibrils in collagen microstructure is also known from two-dimensional light, electron, and X-ray
95 scattering microscopy in tendons and other collagenous tissues (Reed, Wood and Keech, 1956; Lillie *et al.*, 1977; Altraud *et al.*, 1987; Folkhard *et al.*, 1987; Vidal, 2003; Franchi *et al.*, 2010; Kalson *et al.*, 2012).

Experimental observations and finite element (FE) modeling suggest that helical structures in tendon may have significant mechanical effects. The rotation
100 and high Poisson's ratio observed during tendon's axial loading have been attributed to such structures (Reese, Maas and Weiss, 2010; Thorpe *et al.*, 2013;

Buchanan, Lakes and Vanderby, 2017). Furthermore, some FE models have studied the groups of helical fibrils by combining the fibrils with interfibrillar matrix in a mesh to produce the nonlinear stress response of fascicles (Reese, Maas and Weiss, 2010; Carniel, Klahr and Fancello, 2019). Despite the potential of helical fibril organization to affect tendon's microscale mechanics, little is known about individual groups of helically wrapped fibrils and their mechanical implications. We hypothesized that helical wrapping can induce frictional load transfer between fibrils, allowing for mechanical interfibrillar load transfer without an intermediate matrix. This would imply that friction between helically wrapped fibrils can contribute to load transfer, in addition to interfibrillar matrix shear and fibril fusion/branching.

The scope of this contribution was to visualize the three-dimensional fibril organization of rat tail tendon and to study the potential of interfibrillar friction within helically wrapped groups of fibrils to serve as a mechanism for load transfer. First, we visualized the microstructure of tendon in three dimensions using SBF-SEM. We found a complex network, with many helically wrapped fibrils. These observations informed the second part of this study, in which we used finite element (FE) analysis to test the hypothesis that frictional contact between helically wrapped fibrils can transfer stress (load) between fibrils without a need for a mediating matrix. This study elucidates new aspects of tendon microstructure, providing a detailed image of fibril tortuosity, fusion/branching, and organization into helical groups. Importantly, our results

establish interfibrillar friction as a new potential mechanism for interfibrillar load
125 transfer, advancing our knowledge about microscale structure–mechanics relationships.

Methods

Serial block-face SEM imaging

A tail tendon fascicle from a three-month-old male Sprague-Dawley rat
130 was dissected as previously described (Safa *et al.*, 2017), and used for SBF-SEM imaging. To prepare for imaging, the fascicle was placed in PBS for 8 hours to equilibrate and then soaked overnight at 4°C in a solution of 2% glutaraldehyde and 2% paraformaldehyde in 0.1 M sodium cacodylate buffer. The sample was subsequently stained and resin-embedded, according to established techniques
135 (Starborg *et al.*, 2013).

The transverse cross-section was scanned in series under 1.78 kV in low-vacuum pressure with three microseconds dwelling time using an Apreo VolumeScope (Thermo Fisher Scientific, Waltham MA). After the end of the scanning of each section, a 200 nm layer of the block's face was removed by
140 means of a mechanical slicer and the scanning was repeated. The in-plane resolution of the scans was 10 nm/pixel with 432 slices that covers a total volume of (20.27 μm × 16.74 μm × 86.20 μm), where the third dimension is measured along the fascicle's axial direction.

Segmentation and data analysis

145 The SEM images were smoothed using a Gaussian blur filter and a representative subset of fibrils were manually segmented through the entire 3D image stack (Fig. 1A). Only fibrils that spanned the entire image stack were used for analysis ($n = 42$ fibrils). The segmentation was done using Seg3D (seg3d.org). Since the axial distance between subsequent images was small (200

150 nm) the fibrils appear as semi-circular spots that move in-plane allowing for the fibrils to be inspected and tracked through the image stack (Fig. 1A-C).

To confirm that the manually segmented fibrils were a representative selection of all the fibrils, we segmented all fibrils in each of ten equally spaced 2D sections by thresholding (ImageJ, imagej.nih.gov). The distribution of fibril

155 diameter was calculated and compared to that of the manual 3D fibril segmentations (Fig. 1D and E). The distributions matched, confirming that the manually segmented fibrils were a representative sample. The manual 3D fibril segmentations were used for all subsequent analysis.

To determine the variation in fibril diameter along the length, we calculated

160 the normalized diameter of each fibril in each section in the image stack. The normalized diameter for a fibril at section i is defined as

$$\bar{d}(z_i) = \frac{d(z_i)}{\tilde{d}}, \tag{1}$$

where z_i is the scan depth, $d(z_i) = \sqrt{4A_i/\pi}$ is the diameter of the fibril, A_i is the cross-sectional area of the fibril, and $\tilde{d}$ is the median of $d(z_i)$ across all sections

(Fig. 1C). To quantify the complexity of the fibrillar network, we calculated the
165 percent tortuosity for each fibril as

$$\tau = \left(\frac{\sum_{i=1}^{N-1} s_i}{l_0} - 1 \right) \times 100; \tag{2}$$

here, l_0 is the end-to-end distance of the fibrils, and s_i is the distance between fibril centroids in adjacent sections, and N is the number of sections (Fig. 1C). Approximately half of the segmented fibrils ($n = 20$) were in helical groups; for these fibrils we calculated the pitch (λ) by diving the total scan depth (86.20 μm)
170 by the number of turns in the helices.

Statistics

The variation in diameter along the length was tested by calculating, for each section, the 95% confidence interval of normalized diameter (Eq. 1) across the fibrils in that section. To test the correlation between fibril diameter and
175 tortuosity, we conducted a linear regression analysis between $\tilde{d}$ and τ using Pearson's correlation method. Statistical significance was defined as $p < 0.05$.

Finite element analysis of helical fibril structures

Helical wrapping of fibrils around each other was a commonly observed feature, and we hypothesized that this helical wrapping may provide interfibrillar
180 load transfer. To study this, we developed a three-dimensional finite element (FE) model of a pair of helical fibrils in contact (Fig. 1F and G) using FEBio software (FEBio2.8 febio.org) (Maas *et al.*, 2012). The fibril diameter was taken to be 200

nm, and according to our observations from SBF-SEM, the helix pitch was set at 40 μm. The entire model included three full fibril revolutions (i.e., $L = 3\lambda$ where L is the total length). The boundary condition was set as that each fibril had one free-end. In one fibril, the opposite end was anchored; in the other fibril, it was set to move to create 8% axial strain (Fig. 1F). The value of 8% was selected from experimental data as the maximum tissue strain prior to failure (Lee *et al.*, 2017).

We used an isotropic compressible neo-Hookean constitutive relation for the fibrils (Bonet and Wood, 1997):

$$\Psi(I_1, J) = \frac{E}{4(1+\nu)}(I_1 - 3) - \frac{E}{2(1+\nu)}\ln J + \frac{E\nu}{2(1+\nu)(1-2\nu)}(\ln J)^2. \quad (3)$$

Where, Ψ is the strain energy, I_1 is the first invariant of the right Cauchy-Green strain tensor and J is the Jacobian of deformation; E is the Young's modulus, and ν is the Poisson's ratio. The model parameters were set as $E = 1\ \mathrm{GPa}, \nu = 0.2$. The friction parameter between fibrils was set as $\mu = 0.5$, and the helix pitch was set as $\lambda = 40$ μm.

To solve the frictional contact problem between the fibrils we employed the penalty method regularized with an augmented Lagrangian scheme that has been implemented in FEBio (Zimmerman and Ateshian, 2018). In the initial configuration the fibrils were in contact along the entire length. We used a mesh consisting of 20,160 hexahedral trilinear elements and 23,478 nodes based on a mesh sensitivity analysis (Fig 1G). To improve the stability of the contact

algorithm we used a frictionless external cylindrical sheath with a weak modulus (10% of fibril modulus) to prevent separation in the intermediate steps of the iterative FE solver. The sheath was highly effective in increasing the stability of the model, and did not alter the final solutions. This was confirmed by using different moduli for the sheath between 0.1% and 1000% of the fibril modulus; the same mechanical response was produced in each case.

The reaction force at the anchored end of the fixed fibril was divided by the cross sectional area and used as the measure for load transfer. To assess the sensitivity of the load transfer, we performed a one-at-a-time parametric sensitivity analysis by varying the model parameters in a range according to the reported values in the literature for fibril properties that are summarize in Table 1 (Wenger *et al.*, 2007; Minary-Jolandan and Yu, 2009; Gautieri *et al.*, 2011; Yang *et al.*, 2012; Chung *et al.*, 2013; Szczesny and Elliott, 2014b; Wells *et al.*, 2015; Liu, Ballarini and Eppell, 2016). Since the experimental data for frictional coefficient of fibril-on-fibril is not available, we used an estimated range ($0 < \mu < 2$) based on AFM indentation tests (Chung *et al.*, 2013). We studied the following cases by changing one parameter at a time: $E = 0.1$ to10 GPa,$\nu =$ 0 to 0.4, $\mu = 0$ to 2, $\lambda = 20$ to 80 μm.

To evaluate the spatial distribution of the induced stress and deformation in the fibrils we plotted axial stress and we also plotted the normalized displacement ($\overline{u}$) relative to the mid-section of each fibril along the axial direction. We defined normalized displacement as

$$\bar{u}(z) = \frac{1}{\lambda}\left(u(z) - u\left(\frac{L}{2}\right)\right). \quad (4)$$

225 Here, $u(z)$ is the axial displacement at position z along the fibril length.

Results

Microstructure of fibrils and SBF-SEM

To describe the microstructure of tendon, we segmented fibrils from the SBF-SEM images in three-dimensions. The segmentation indicated that although
230 the fibrils are mostly axially-aligned, they create a complex network around the cells (Fig. 2A). From the manually segmented fibrils we quantified the fibril diameter throughout the scan depth (Eq. 1) and the percent tortuosity (Eq. 2). As expected, the fibrils' diameter did not vary along the fibril length (Fig. 2B), which is consistent with previous findings (Svensson *et al.*, 2017). Note that the
235 normalized fibril diameter (Eq. 1) was not significantly different than one across the scan depth (Fig 2B). This observation supports the use of a single median diameter value assigned to each fibril for correlation with the tortuosity. We quantified the % tortuosity (τ) of each segmented fibril (Eq. 2), and calculated its correlation with the median diameter of the fibrils. This showed that for all of the
240 fibrils, τ was small ($< 1\%$) and it had a weak correlation with the diameter ($r = -0.36, p < 0.05$) (Fig. 2C). As a result, the smaller fibrils are more likely to have higher tortuosity, and thus have a more complex structure. For the tortuosity

analysis, one fibril that made a right-angle turn and passed through the cell membrane (Fig. 3C, discussed below) was not included in the correlation.

We made several isolated structural observations that have potential mechanical implications: tapered fibril end (Fig. 3A and Supplementary Video 1), fibril fusion/branching (Fig. 3B and Supplementary Video 2), and one fibril that wrapped around the cells (Fig. 3C and Supplementary Video 3). For the tapered fibril end, in the last ~4 μm of the fibril length (scan depth of 38-42 μm) a reduction in fibril diameter was evident, where the fibril gradually fades away in the image sequence when approaching from the deeper scanned layers (Fig. 3A). At the fusion/branching site, a small fibril merges with a larger one, and in the subsequent scanned images the larger resulting fibril branches into two distinct ones. The fusion/branching site approximately spanned 6 μm, where at least two fibrils were not distinguishable (Fig. 3B). Another interesting feature was one fibril that made almost a full turn around the cells (Fig. 3C). These features were interesting but were isolated observations in the dataset.

When looking at the axial view of the fibrils, we observed several helical structures (Fig. 4 and Supplementary Video 4). In particular, many fibrils locally wrapped around each other, which contained two, three, or more fibrils with both left and right-handed helical configuration (Fig. 4 and Supplementary Video 5). Almost 50% (20 out of 42 fibril) of the fibrils that we segmented were in helical groups, although the sampling was not purely random. Of these helical fibrils, 13 fibrils had a right-handed twist and 7 were left-handed (Fig. 4B). These fibrils

265 made an average of 2.2 ± 1.4 turns around each other along the scan-length (Fig. 4C), that also corresponds to an overall $\sim 39 \pm 18$ μm helical pitch (λ, the axial length of one full turn as described in Fig. 1F).

Finite element simulations of the helical fibrils

We used a finite element model to test our hypothesis that frictional contact
270 between helically wrapped fibrils can transfer stress (load) between fibrils without a need for a mediating matrix. The stress transfer was proportional to the fibril's tensile modulus (Fig. 5A). Further parametric studies indicated that there is no change to the transferred stress with a change in Poisson's ratio (ν) (Fig. 5B). As expected, the transferred load increased with an increase of frictional
275 coefficient (μ) (Fig. 5C). Our results show that the load transfer decreased with an increase in pitch (λ) (Fig. 5D).

To evaluate the spatial distribution of stress and deformation along the length of each fibril and its dependence on the friction coefficient, we plotted the axial stress and axial displacement ($\overline{u}$, Eq. 4) at the end of loading (Fig. 6). The
280 fibril stress was zero with no friction ($\mu = 0$, Fig. 6B) and it increased with higher friction coefficient (Fig. 6C and D). The axial stress varied linearly along the length of the fibril, increasing with distance from the free boundary and the stress in each fibril was the mirror image of the stress in the other one (Fig. 6A-D), which is in accordance with the static equilibrium condition. Similarly, for the
285 fibril deformation, in the zero friction case, there was no axial deformation, hence

the fibrils slid freely (Fig. 6E). When friction was increased, the induced deformation also increased, showing a plateau at the free ends indicating no strain, which confirms the stress-free boundary condition imposed on the model (Fig. 6F and G).

290 ## Discussion

In this study, we visualized the microscale structure of tendon fibrils in three dimensions using serial block-face scanning electron microscopy (SBF-SEM) and studied the mechanical implications of helical fibrils as a mechanism for interfibrillar load transfer using FE analysis. We found that tendon fibrils are
295 not purely parallel structures and there are many helical fibrils that wrap around each other and in groups. Our FE analysis indicated that, in addition to other potential mechanisms of load transfer (interfibrillar matrix and fusion/branching of smaller fibrils), the helical fibrils can also mediate load transfer through frictional mechanical contact.

300 ### Microstructure of fibrils and SBF-SEM

We observed helical structures that twisted around each other (Fig. 4). The existence of helical fibrils was previously reported, which were suggested to be left-handed (Franchi *et al.*, 2010); however, our findings showed a similar number of the left-handed and right-handed helical fibrils (Fig. 4B). These helical
305 structures explain the rotation of tendon in tension (Buchanan, Lakes and Vanderby, 2017). Additionally, they have been used as an explanation for the

macro-scale mechanical behavior of tendon, in particular for the low stiffness at small deformations and the large tensile Poisson's ratio (Reese, Maas and Weiss, 2010; Thorpe *et al.*, 2013). The grouping of fibrils into helices can mediate load transfer by inducing frictional contact between fibrils during axial loading.

We observed some interesting but isolated features that can have implications for load transfer and loading on cells. For load transfer, we observed a tapered fibril end and fusion/branching, which agree with previous findings (Svensson *et al.*, 2017), with the difference that the tapered end in this study was observed in a "straight" fibril in contrast to the hairpin shape in the previous study. As previously suggested by Szczesny and co-workers (Szczesny *et al.*, 2017), an instance of fusion/branching, such as the one described above, could mediate load transfer between fibrils via direct physical connection. A free fibril end like the tapered end can also mediate load transfer by allowing interfibrillar sliding and shear stress, which is a well-documented phenomenon in experimental studies (Thorpe *et al.*, 2013; Szczesny and Elliott, 2014b; Lee *et al.*, 2017). Additionally, we observed a fibril that wrapped around the cells, which indicates that during an axial loading, lateral compression can be exerted on the cells affecting tendon mechanotransduction (Lavagnino *et al.*, 2015).

The fibril structure assessment was subject to some limitations. The SBF-SEM technique generates large 3D datasets and segmentation is consequently difficult compared to 2D SEM, creating practical limitations in data collection and analysis (Svensson *et al.*, 2017). Although we consequently chose to do in-

depth manual segmentation for only one sample, we performed several scans of additional fascicles, and these scans showed similar structural features. A separate limitation is that our observations only included a region near the tenocytes, and other regions further away from the cells might have a different structure. Furthermore, we only scanned the tail tendon, which is a low-stress tendon; further investigation is needed to confirm the existence of helical fibril groups in other tendons.

Finite element simulations of the helical fibrils

Interfibrillar load transfer by friction in a helical contact does not require interfibrillar matrix bonding, but the sum of its contribution over many fibrils and its relative magnitude in comparison to other load transfer mechanisms such as chemical bonding remains unknown. Here, the estimated magnitude of the transferred fibril stress ($\sim 0.2 - 4$ MPa) was low compared to the ultimate stress of the fibrils—typically in the range of 90 MPa (Liu, Ballarini and Eppell, 2016). The large variation in mechanical parameters of fibrils (Table 1) and the unknown accumulation among hundreds of fibrils hinders accurate calculation of the total load transferred in situ by the interfibrillar friction mechanism. Of particular importance, the fibril-on-fibril friction coefficient is unavailable. Thus, more experimental measurements of single fibrils and groups of fibrils are needed for more accurate estimations.

The variations in fibril stress transfer and displacement observed in the parametric FE sensitivity analysis make physical sense (Fig. 6). In particular, the

dependence of transferred stress with modulus and frictional coefficient are expected based on Hooke's law and Coulomb's friction law, respectively, and they were shown using our FE model (Fig. 5A and C). The decrease in reaction force by increasing the pitch of the helix, which is shown in Fig. 5D, can be explained by a reduction in lateral compression (normal force) on the fibrils as the pitch angle decreases and the fibrils become more parallel. The lack of dependence on Poisson's ratio was an unexpected observation that might be due to the high aspect ratio of the fibril's geometry or due to the isotropy of the constitutive relation (Fig. 5B). Large Poisson's ratio in tension ($\nu \sim 2$) have been reported for individual fibrils (Wells *et al.*, 2015), which is greater than the isotropic limit of $\nu = 0.5$. Anisotropy of the isolated fibril material might need to be incorporated in the future to further investigate the effect of Poisson's ratio in the interfibrillar load transfer. The curves in Fig. 5 were not smooth, which is potentially related to the nature of frictional contact that can switch between slip and stick conditions and cause jitter (imagine moving heavy house furniture on ceramic), however the trends are clear, and this does not affect the outcome of the sensitivity analysis.

Interfibrillar friction causes a gradient of axial stress in the fibril. In the simulated cases (Fig 6), the spatial distribution of stress variation and deformation match the distributions of stress and deformation based on established shear-lag theories as applied to tendon fibrils (Szczesny and Elliott, 2014a). Interfibrillar load transfer and sliding requires free fibril ends that is observed in experiments,

regardless of whether the interfibrillar load transfer mechanism is extrafibrillar matrix shear lag or interfibrillar friction (Provenzano and Vanderby, 2006; Svensson *et al.*, 2017; Szczesny *et al.*, 2017). This justifies the assumption of free fibril ends in the FE model. Free fibril ends may exist in the form of tapered ends (such as Fig. 3A) or a weak link along the fibril length that can act as an effective fibril end due to its high compliance (Veres, Harrison and Lee, 2014). However, it is not yet clear which form is structurally more common. Although based on our findings and prior studies tapered ends and fusion/branching sites are not likely to be common features in mature tendon (Provenzano and Vanderby, 2006; Svensson *et al.*, 2017), they may still have a role in load transfer, and further investigations are required to explore these microstructures.

In conclusion, we used SBF-SEM to visualize the three-dimensional microscale tendon structure of the fibrillar network, and used FE analysis to demonstrate that helically arranged fibrils can have the mechanical function of frictional interfibrillar load transfer. Interfibrillar friction should be considered as another potential mechanism for interfibrillar load transfer, in addition to the previously postulated mechanisms of interfibrillar matrix shear and direct load transfer through fibril junctions. This study shows that a combined approach of SBF-SEM imaging and FE modeling is a powerful tool to study structure-mechanics relationships in tendon microstructure.

Conflict of interest

The authors do not have any conflict of interests to disclose.

395 **Acknowledgments**

We would like to acknowledge Bioimaging center in the Delaware Biotechnology Institute (DBI) and the Thermo Fisher Scientific Company for SBF-SEM imaging. The funding for this study was made available from NIH-NIBIB grant R01-EB002425. Microscopy access was supported by grants from
400 the NIH-NIGMS (P20 GM103446), the NSF (IIA-1301765) and the State of Delaware. The content is solely the responsibility of the authors and does not necessarily represent the official views of the NIH.

Appendix: Supplementary dataset

The image stack for SBF-SEM images are available at (Safa *et al.*, 2019).

405 **References**

Ahmadzadeh, H., Connizzo, B. K., Freedman, B. R., Soslowsky, L. J. and Shenoy, V. B. (2013) 'Determining the contribution of glycosaminoglycans to tendon mechanical properties with a modified shear-lag model.', *Journal of biomechanics*, 46(14), pp. 2497–503. doi: 10.1016/j.jbiomech.2013.07.008.

410 Altraud, W., Daniela, F., Hristm Ann, C., Erner, W., Eercken, G., Knörzer, E., Koch, M. H. J. J., Mosler, E., Emetschek-Gansler, H. N., Nemetschek, T., Folkhard, W., Koch, M. H. J. J., Geercken, W., Knörzer, E., Mosler, E.,

Nemetschek-Gansler, H. and Nemetschek, T. (1987) ‘Twisted Fibrils are a Structural Principle in the Assembly of Interstitial Collagens, Chordae Tendineae Included’, *Z. Naturforsch*, 42(11–12), pp. 1303–1306. doi: 10.1515/znc-1987-11-1225.

Bonet, J. and Wood, R. D. (1997) *Nonlinear Continuum Mechanics for Finite Element Analisys*. Cambridge University Press. Available at: https://books.google.com/books?id=ORmLdrq1fI8C.

Buchanan, K. A., Lakes, R. S. and Vanderby, R. (2017) ‘Chiral behavior in rat tail tendon fascicles’, *Journal of Biomechanics*. Elsevier, 64, pp. 206–211. doi: 10.1016/j.jbiomech.2017.09.034.

Carniel, T. A., Klahr, B. and Fancello, E. A. (2019) ‘On multiscale boundary conditions in the computational homogenization of an RVE of tendon fascicles’, *Journal of the Mechanical Behavior of Biomedical Materials*, 91, pp. 131–138. doi: 10.1016/j.jmbbm.2018.12.003.

Chung, K. H., Chen, A. K., Anderton, C. R., Bhadriraju, K., Plant, A. L., Bush, B. G., Cook, R. F. and Delrio, F. W. (2013) ‘Frictional properties of native and functionalized type i collagen thin films’, *Applied Physics Letters*. American Institute of Physics, 103(14), p. 143703. doi: 10.1063/1.4824685.

Fessel, G. and Snedeker, J. G. (2009) ‘Evidence against proteoglycan mediated collagen fibril load transmission and dynamic viscoelasticity in tendon.’, *Matrix biology : journal of the International Society for Matrix Biology*, 28(8), pp. 503–10. doi: 10.1016/j.matbio.2009.08.002.

435 Folkhard, W., Koch, M. H. J., Geercken, W., Knörzer, E., Mosler, E., Nemetschek-Gansler, H. and Nemetschek, T. (1987) 'Twisted fibrils are a structural principle in the assembly of interstitial collagens, chordae tendineae included', *Zeitschrift fur Naturforschung - Section C Journal of Biosciences*, 42(11–12), pp. 1303–1306. doi: 10.1515/znc-1987-11-1225.

440 Franchi, M., Ottani, V., Stagni, R. and Ruggeri, A. (2010) 'Tendon and ligament fibrillar crimps give rise to left-handed helices of collagen fibrils in both planar and helical crimps', *Journal of Anatomy*, 216(3), pp. 301–309. doi: 10.1111/j.1469-7580.2009.01188.x.

Gautieri, A., Vesentini, S., Redaelli, A. and Buehler, M. J. (2011) 445 'Hierarchical structure and nanomechanics of collagen microfibrils from the atomistic scale up', *Nano Letters*, 11(2), pp. 757–766. doi: 10.1021/nl103943u.

Hashimoto, T., Thompson, G. E., Zhou, X. and Withers, P. J. (2016) '3D imaging by serial block face scanning electron microscopy for materials science using ultramicrotomy', *Ultramicroscopy*. North-Holland, 163, pp. 6–18. doi: 450 10.1016/J.ULTRAMIC.2016.01.005.

Kalson, N. S., Lu, Y., Taylor, S. H., Starborg, T., Holmes, D. F. and Kadler, K. E. (2015) 'A structure-based extracellular matrix expansion mechanism of fibrous tissue growth', *eLife*, 4. doi: 10.7554/eLife.05958.

Kalson, N. S., Malone, P. S. C., Bradley, R. S., Withers, P. J. and Lees, V. 455 C. (2012) 'Fibre bundles in the human extensor carpi ulnaris tendon are arranged in a spiral', *Journal of Hand Surgery (European Volume)*. SAGE

PublicationsSage UK: London, England, 37(6), pp. 550–554. doi: 10.1177/1753193411433228.

Kannus, P. (2000) ‘Structure of the tendon connective tissue’, *Scandinavian Journal of Medicine and Science in Sports*, 10(6), pp. 312–320. doi: 10.1034/j.1600-0838.2000.010006312.x.

Kastelic, J., Galeski, A. and Baer, E. (1978) ‘The Multicomposite Structure of Tendon’, *Connective Tissue Research*, 6(1), pp. 11–23. doi: 10.3109/03008207809152283.

Lavagnino, M., Wall, M. E., Little, D., Banes, A. J., Guilak, F. and Arnoczky, S. P. (2015) ‘Tendon mechanobiology: Current knowledge and future research opportunities.’, *Journal of orthopaedic research : official publication of the Orthopaedic Research Society*, 33(6), pp. 813–22. doi: 10.1002/jor.22871.

Lee, A. H., Szczesny, S. E., Santare, M. H. and Elliott, D. M. (2017) ‘Investigating mechanisms of tendon damage by measuring multi-scale recovery following tensile loading’, *Acta Biomaterialia*, 57, pp. 363–372. doi: 10.1016/j.actbio.2017.04.011.

Lillie, J. H., MacCallum, D. K., Scaletta, L. J. and Occhino, J. C. (1977) ‘Collagen structure: Evidence for a helical organization of the collagen fibril’, *Journal of Ultrasructure Research*, 58(2), pp. 134–143. doi: 10.1016/S0022-5320(77)90025-9.

Liu, Y., Ballarini, R. and Eppell, S. J. (2016) ‘Tension tests on mammalian collagen fibrils’, *Interface Focus*, 6(1), p. 20150080. doi:

10.1098/rsfs.2015.0080.

480 Maas, S. A., Ellis, B. J., Ateshian, G. A. and Weiss, J. A. (2012) 'FEBio: Finite Elements for Biomechanics', *Journal of Biomechanical Engineering*, 134(1), p. 011005. doi: 10.1115/1.4005694.

Minary-Jolandan, M. and Yu, M. F. (2009) 'Nanomechanical heterogeneity in the gap and overlap regions of type I collagen fibrils with
485 implications for bone heterogeneity', *Biomacromolecules*, 10(9), pp. 2565–2570. doi: 10.1021/bm900519v.

Pensalfini, M., Duenwald-Kuehl, S., Kondratko-Mittnacht, J., Lakes, R. and Vanderby, R. (2014) 'Evaluation of global load sharing and shear-lag models to describe mechanical behavior in partially lacerated tendons.', *Journal of*
490 *biomechanical engineering*, 136(9), p. 091006. doi: 10.1115/1.4027714.

Pingel, J., Lu, Y., Starborg, T., Fredberg, U., Langberg, H., Nedergaard, A., Weis, M., Eyre, D., Kjaer, M. and Kadler, K. E. (2014) '3-D ultrastructure and collagen composition of healthy and overloaded human tendon: evidence of tenocyte and matrix buckling', *Journal of Anatomy*, 224(5), pp. 548–555. doi:
495 10.1111/joa.12164.

Provenzano, P. P. and Vanderby, R. J. (2006) 'Collagen fibril morphology and organization: implications for force transmission in ligament and tendon.', *Matrix biology : journal of the International Society for Matrix Biology*. Netherlands, 25(2), pp. 71–84. doi: 10.1016/j.matbio.2005.09.005.

500 Redaelli, A., Vesentini, S., Soncini, M., Veres, S. P., Mantero, S. and

Montevecchi, F. M. (2003) 'Possible role of decorin glycosaminoglycans in fibril to fibril force transfer in relative mature tendons—a computational study from molecular to microstructural level', *Journal of Biomechanics*, 36(10), pp. 1555–1569. doi: 10.1016/S0021-9290(03)00133-7.

Reed, R., Wood, M. J. and Keech, M. K. (1956) 'Helical Nature of the Collagen Fibril', *Nature*. Nature Publishing Group, 177(4511), pp. 697–699. doi: 10.1038/177697a0.

Reese, S. P., Maas, S. A. and Weiss, J. A. (2010) 'Micromechanical models of helical superstructures in ligament and tendon fibers predict large Poisson's ratios.', *Journal of biomechanics*. United States, 43(7), pp. 1394–400. doi: 10.1016/j.jbiomech.2010.01.004.

Safa, B. N., Meadows, K. D., Szczesny, S. E. and Elliott, D. M. (2017) 'Exposure to buffer solution alters tendon hydration and mechanics', *Journal of Biomechanics*. Elsevier, 61, pp. 18–25. doi: 10.1016/j.jbiomech.2017.06.045.

Safa, B. N., Peloquin, J. M., Natriello, J. R., Caplan, J. L. and Elliott, D. M. (2019) 'Cross-sectional serial block-face images of rat tail tendon fascicle'. doi: 10.5281/ZENODO.2560801.

Screen, H. R. C., Shelton, J. C., Chhaya, V. H., Kayser, M. V., Bader, D. L. and Lee, D. A. (2005) 'The Influence of Noncollagenous Matrix Components on the Micromechanical Environment of Tendon Fascicles', *Annals of Biomedical Engineering*, 33(8), pp. 1090–1099. doi: 10.1007/s10439-005-5777-9.

Snedeker, J. G. and Foolen, J. (2017) 'Tendon injury and repair – A perspective on the basic mechanisms of tendon disease and future clinical therapy', *Acta Biomaterialia*. Elsevier, 63, pp. 18–36. doi: 10.1016/J.ACTBIO.2017.08.032.

Starborg, T. and Kadler, K. E. (2015) 'Serial block face-scanning electron microscopy: A tool for studying embryonic development at the cell-matrix interface', *Birth Defects Research Part C - Embryo Today: Reviews*. Wiley-Blackwell, 105(1), pp. 9–18. doi: 10.1002/bdrc.21087.

Starborg, T., Kalson, N. S., Lu, Y., Mironov, A., Cootes, T. F., Holmes, D. F. and Kadler, K. E. (2013) 'Using transmission electron microscopy and 3View to determine collagen fibril size and three-dimensional organization', *Nature Protocols*, 8(7), pp. 1433–1448. doi: 10.1038/nprot.2013.086.

Svensson, R. B., Herchenhan, A., Starborg, T., Larsen, M., Kadler, K. E., Qvortrup, K., Magnusson, S. P., Peter Magnusson, S. and Magnusson, S. P. (2017) 'Evidence of structurally continuous collagen fibrils in tendons', *Acta Biomaterialia*. Acta Materialia Inc., 50, pp. 293–301. doi: 10.1016/j.actbio.2017.01.006.

Szczesny, S. E., Edelstein, R. S. and Elliott, D. M. (2014) 'DTAF dye concentrations commonly used to measure microscale deformations in biological tissues alter tissue mechanics.', *PloS one*. United States: Public Library of Science, 9(6), p. e99588. doi: 10.1371/journal.pone.0099588.

Szczesny, S. E. and Elliott, D. M. (2014a) 'Incorporating plasticity of the

545 interfibrillar matrix in shear lag models is necessary to replicate the multiscale mechanics of tendon fascicles', *Journal of the Mechanical Behavior of Biomedical Materials*. Elsevier, 40, pp. 325–338. doi: 10.1016/j.jmbbm.2014.09.005.

Szczesny, S. E. and Elliott, D. M. (2014b) 'Interfibrillar shear stress is the
550 loading mechanism of collagen fibrils in tendon', *Acta Biomaterialia*. England: Elsevier BV, 10(6), pp. 2582–2590. doi: 10.1016/j.actbio.2014.01.032.

Szczesny, S. E., Fetchko, K. L., Dodge, G. R. and Elliott, D. M. (2017) 'Evidence that interfibrillar load transfer in tendon is supported by small diameter fibrils and not extrafibrillar tissue components', *Journal of Orthopaedic*
555 *Research*, 35(10), pp. 2127–2134. doi: 10.1002/jor.23517.

Thorpe, C. T., Klemt, C., Riley, G. P., Birch, H. L., Clegg, P. D. and Screen, H. R. C. (2013) 'Helical sub-structures in energy-storing tendons provide a possible mechanism for efficient energy storage and return', *Acta Biomaterialia*. Acta Materialia Inc., 9(8), pp. 7948–7956. doi:
560 10.1016/j.actbio.2013.05.004.

Veres, S. P., Harrison, J. M. and Lee, J. M. (2014) 'Mechanically overloading collagen fibrils uncoils collagen molecules, placing them in a stable, denatured state', *Matrix Biology*. doi: 10.1016/j.matbio.2013.07.003.

Vidal, B. de C. (2003) 'Image analysis of tendon helical superstructure
565 using interference and polarized light microscopy', *Micron*. Pergamon, 34(8), pp. 423–432. doi: 10.1016/S0968-4328(03)00039-8.

Wells, H. C., Sizeland, K. H., Kayed, H. R., Kirby, N., Hawley, A., Mudie, S. T. and Haverkamp, R. G. (2015) 'Poisson's ratio of collagen fibrils measured by small angle X-ray scattering of strained bovine pericardium', *Journal of Applied Physics*, 117(4), p. 184905. doi: 10.1063/1.4906325.

Wenger, M. P. E., Bozec, L., Horton, M. A. and Mesquida, P. (2007) 'Mechanical properties of collagen fibrils.', *Biophysical journal*, 93(4), pp. 1255–63. doi: 10.1529/biophysj.106.103192.

Yang, L., van der Werf, K. O., Dijkstra, P. J., Feijen, J. and Bennink, M. L. (2012) 'Micromechanical analysis of native and cross-linked collagen type I fibrils supports the existence of microfibrils', *Journal of the Mechanical Behavior of Biomedical Materials*. Elsevier, 6, pp. 148–158. doi: 10.1016/j.jmbbm.2011.11.008.

Zimmerman, B. K. and Ateshian, G. A. (2018) 'A Surface-to-Surface Finite Element Algorithm for Large Deformation Frictional Contact in febio', *Journal of Biomechanical Engineering*. American Society of Mechanical Engineers, 140(8), p. 081013. doi: 10.1115/1.4040497.

585

Table 1

Table 1: Collagen fibril mechanical properties: Young's modulus (E), Poisson's ratio (ν), frictional coefficient (μ) in tendon unless otherwise noted.

E (GPa)	ν	μ	Method	Tissue	Ref.
0.1 – 10	**0 – 0.4**	**0 – 2**	**-**	**Rat tail**	**Current study's range**
0.326 ± 0.112	-	-	Tensile test MEMS	Rat patellar	(Liu et al., 2016)
0.6 ± 0.2	-	-	Tensile test AFM	Bovine Achilles	(Yang et al., 2012)
0.3 – 1.2	-	-	Atomistic modeling	-	(Gautieri et al., 2011)
1.6 ± 0.4	-	-	Shear-lag curve fitting	Rat tail	(Szczesny and Elliott, 2014)
1.2 – 2.2	-	-	Indentation AFM	Bovine Achilles	(Minary-Jolandan and Yu, 2009)
3.75 – 11.5	0 – 0.5	-	Indentation AFM	Rat tail	(Wenger et al., 2007)
-	2.1 ± 0.7	-	X-ray diffraction	Bovine pericardium	(Wells et al., 2015)
-	-	~ 0.4	Indentation AFM	Collagen film	(Chung et al., 2013)

590

Figure 1

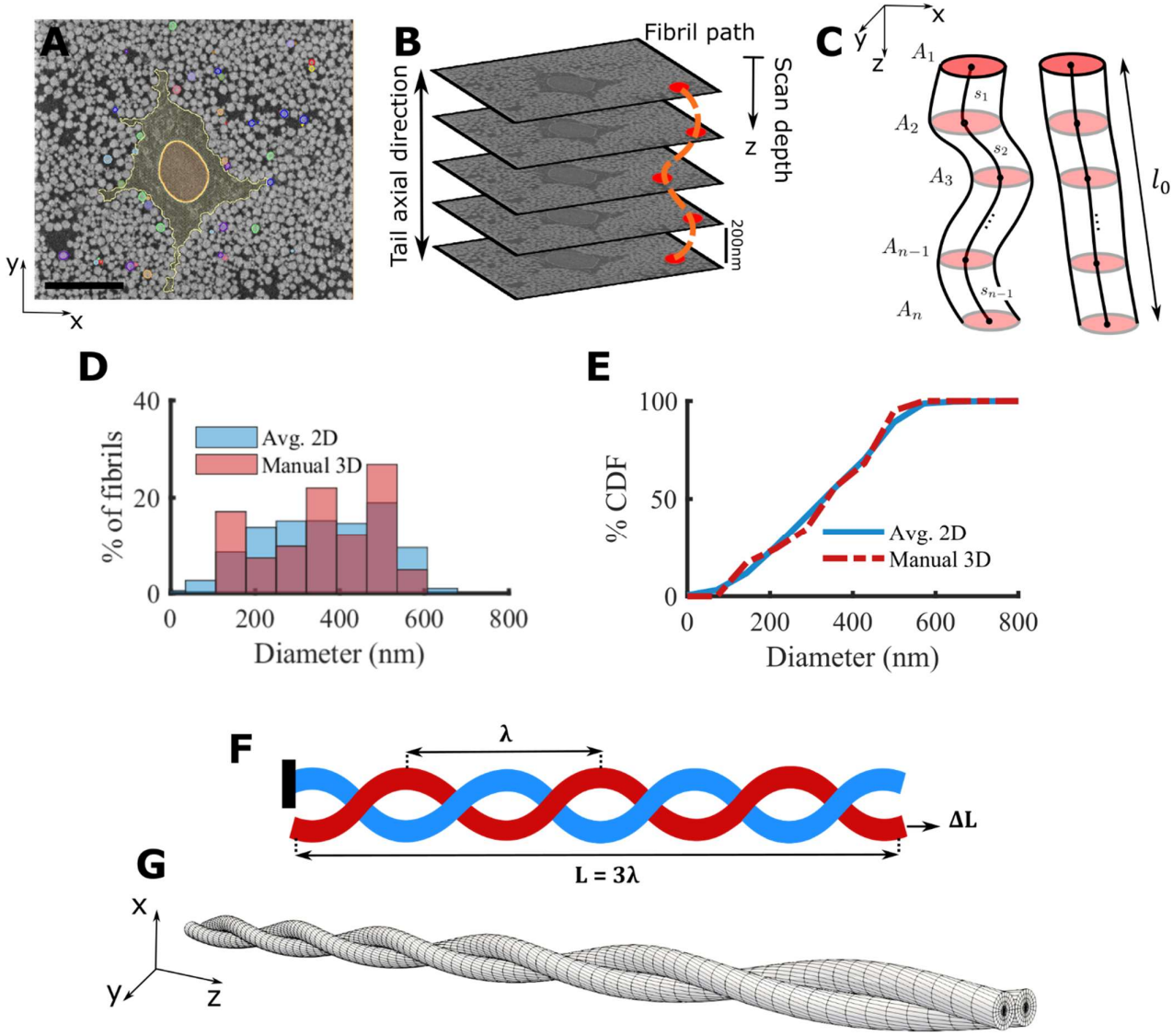

Figure 1: (A) Representative SEM image and in-plane segmentation (scale bar = 5 μm), (B) SBF-SEM imaging process showing sequential stacks of images and a schematic fibril label (dotted orange line) along the tendon length, (C) schematics of fibrils with large (left) and low (right) tortuosity that shows the cross-sectional area (A_i) of fibrils throughout the scan depth and the incremental distance (s_i) between the center of the fibrils. (D) By comparing the distribution and (E) cumulative distribution function (CDF) of the diameter using the averaged 2D automatic segmentation of all fibrils (blue) and the 3D manual segmentation of a subset of 42 fibrils (red), it is evident that the manually segmented fibrils are a representative of the full fibril population. (F) For the finite element analysis a model with three full turns is used ($L = 3\lambda$). The boundary condition is that one fibril (blue) is anchored (left), while the other fibril (red) is pulled in the axial direction (arrow, right) to a deformation of $\Delta L = L\varepsilon$. (G) The mesh used for the finite element simulations shows that the fibrils were initially in contact throughout the length.

Figure 2

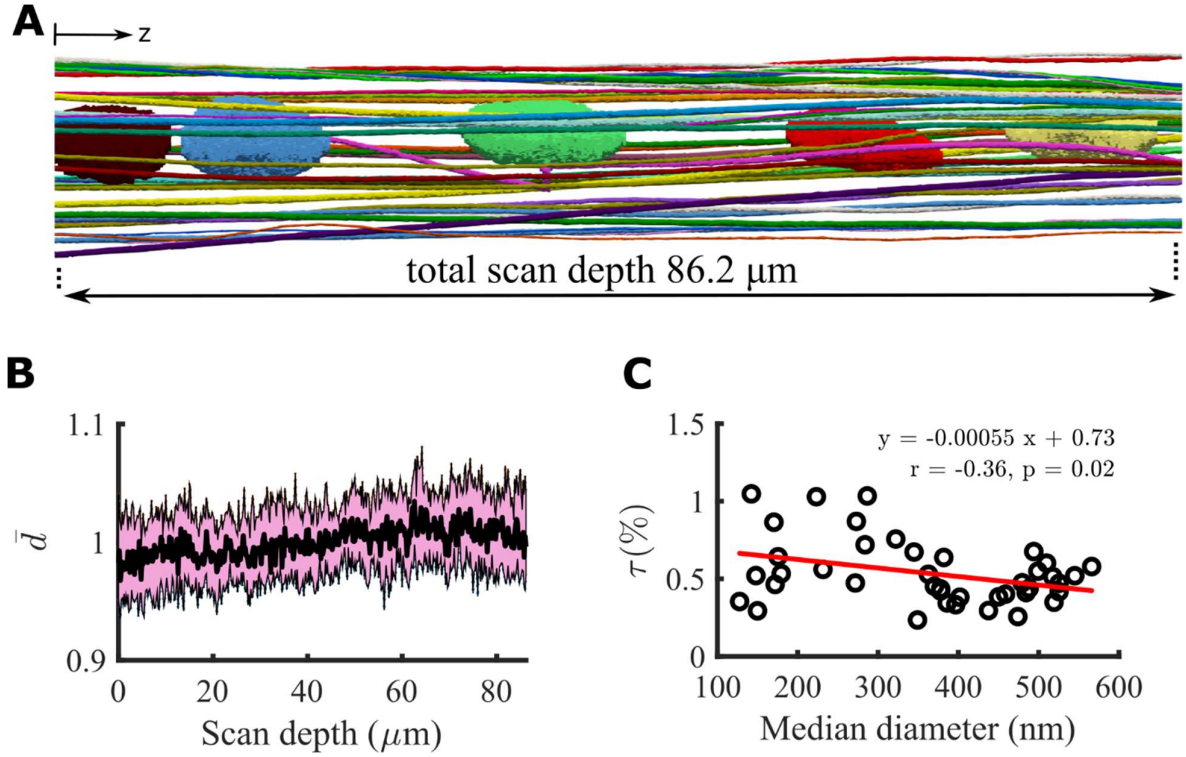

Figure 2: (A) Lateral view of the three dimensional segmentation along the scan length with cell nuclei. Although the fibrils are primarily axially oriented, they have a complex three-dimensional network. (B) the 95% confidence interval (highlighted in pink) of the normalized diameter ($\bar{d}$, Eq. 1) contains the unity value throughout the scan depth, which indicates that the diameter of the fibrils does not change along the scan depth. (C) Percent-tortuosity (τ, Eq. 2) was calculated as a measure of the complexity of the fibrillar structure and is weakly correlated with the median fibril diameter ($r=-0.36$, $p<0.05$).

Figure 3

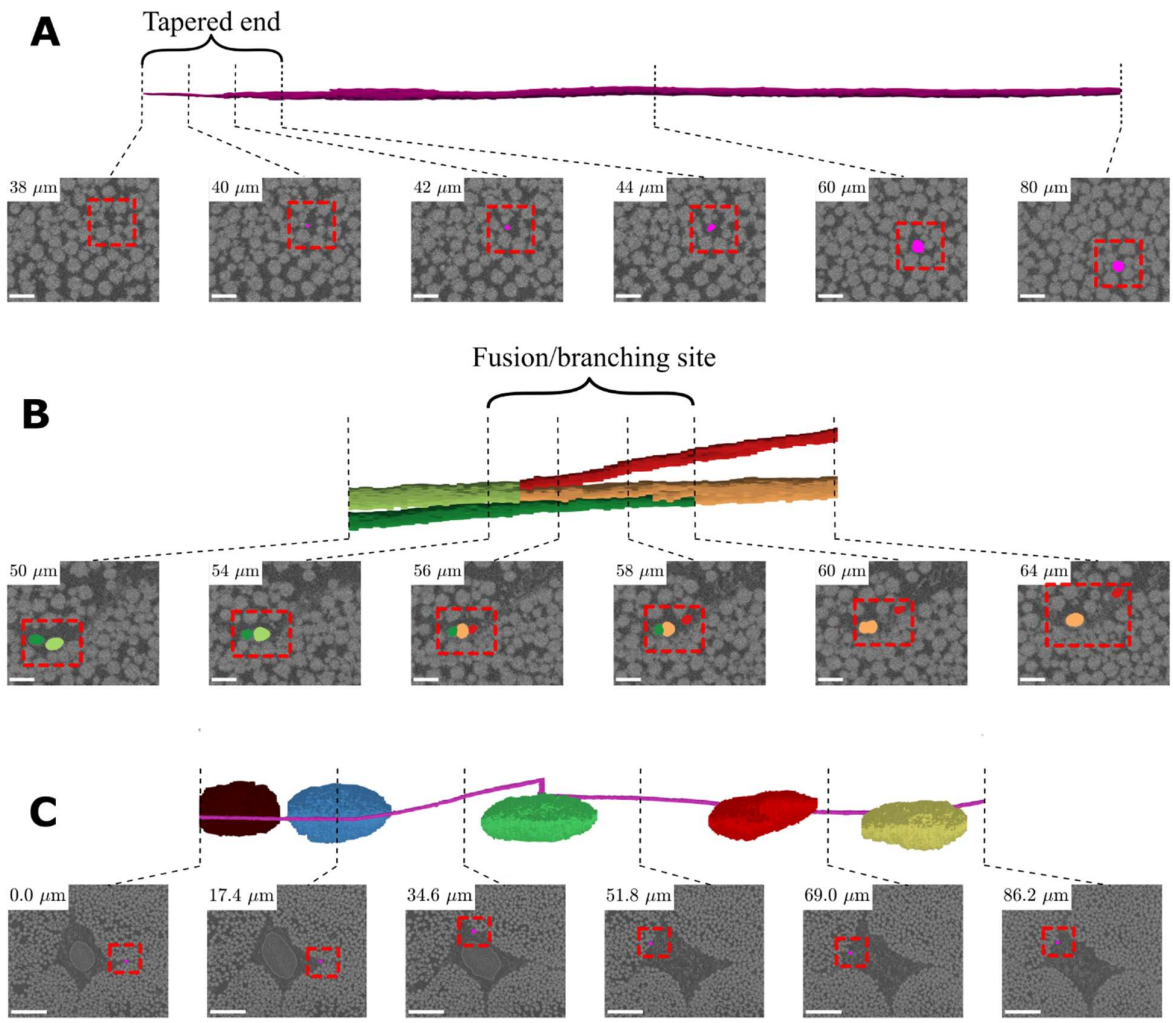

Figure 3: Three interesting but isolated structural features were observed: (A) tapered fibril end (B) fibril fusion/branching and (C) a helical fibril that wrapped around cells (only the nuclei are shown). For each feature, the first row includes the 3D segmentation, and the second row shows the segmentation mask overlaid on the SEM section image (dashed red box). In (A) and (B) scale bar = 1 μm, for (C) scale bar = 5 μm.

Figure 4

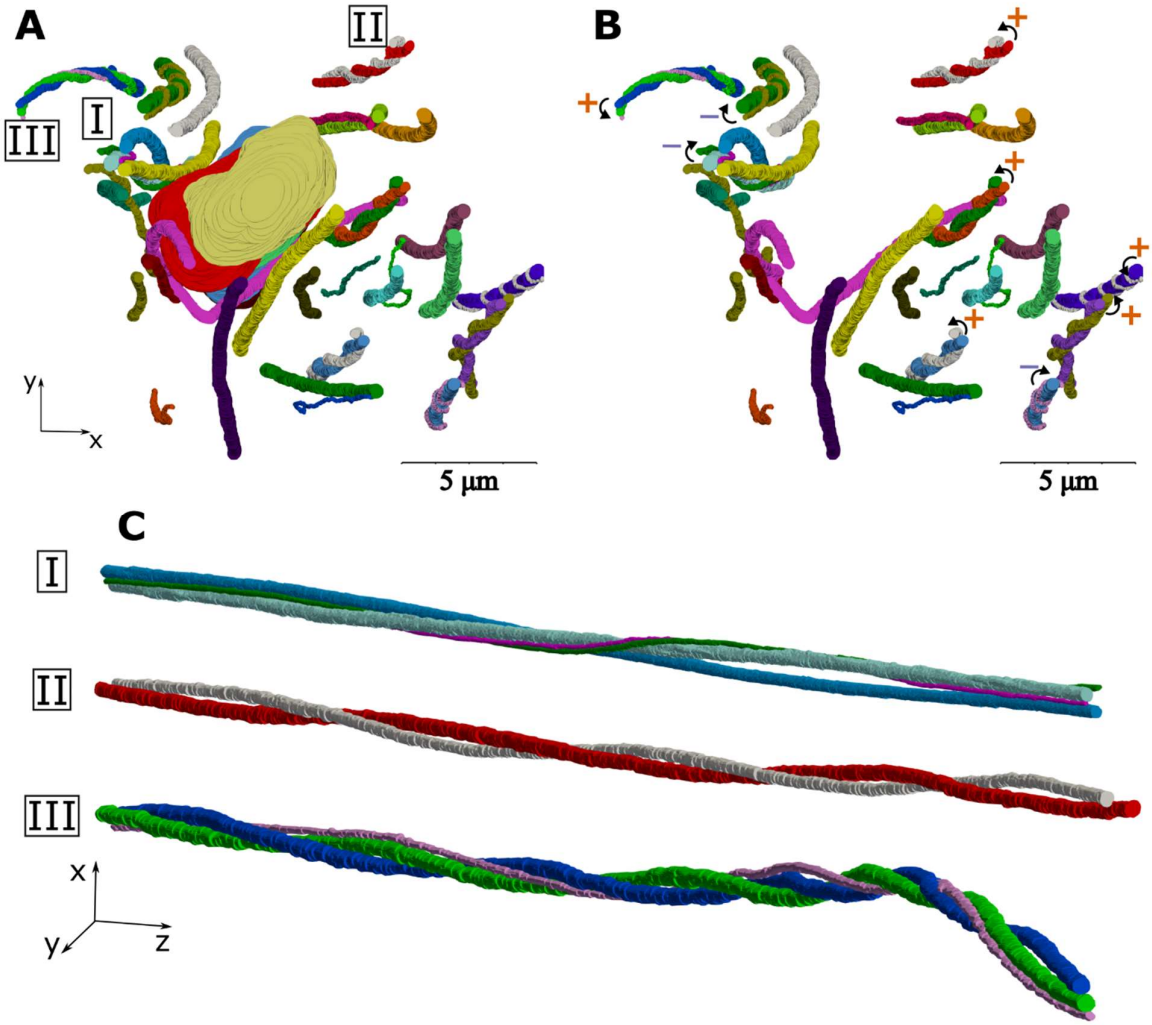

Figure 4: Many helical structures were observed in the axial view of the fibrils that are evident in the figures (A) with and (B) without the cell nuclei. The helical fibril groups have both left (marked with +↺) and right-handed (marked with −↻) twist. (C) Shows three examples of the groups of twisting fibrils with pitch ranging from 20 um to 86 μm.

Figure 5

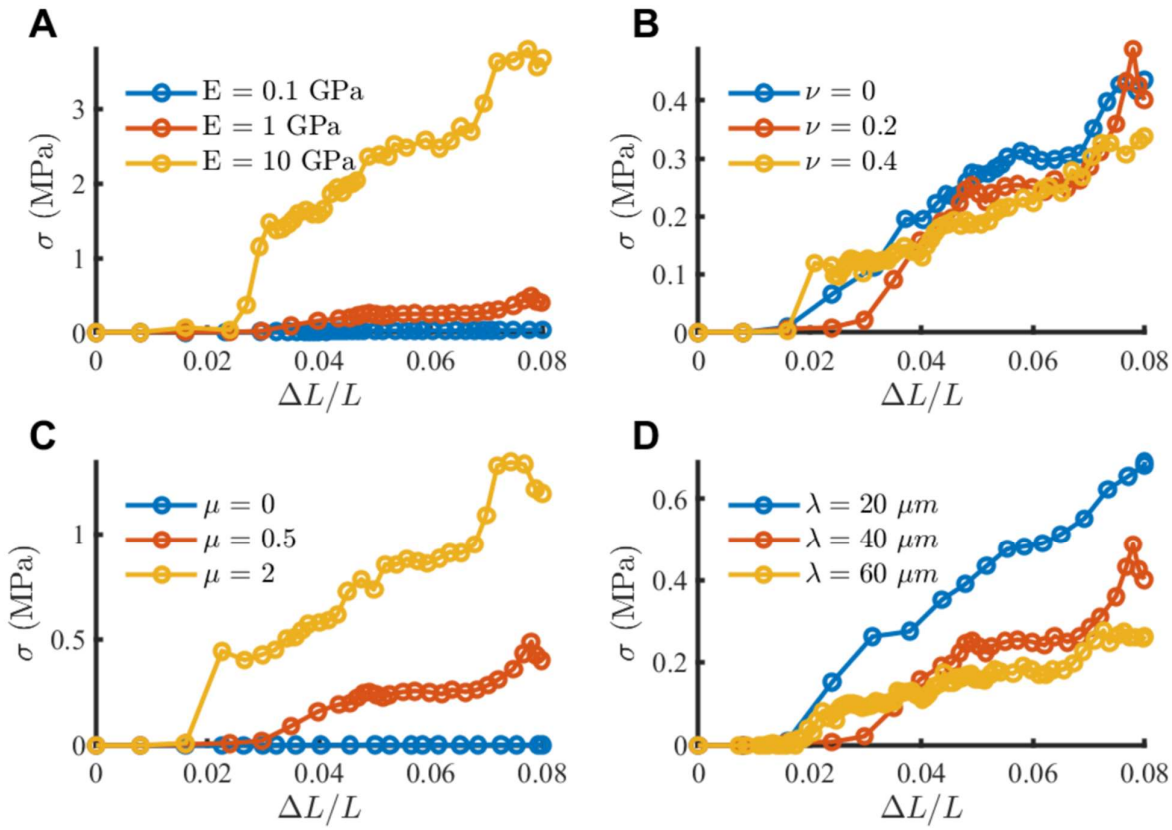

Figure 5: Finite element analysis of stress transfer due to friction between helically grouped fibrils. Base material properties $E = 1$ GPa, $\nu = 0.2, \mu = 0.5$, $\lambda = 40\ \mu m$. The transferred stress (A) increases with fibril modulus E, and (B) is insensitive to Poisson's ratio ν, (C) increases with frictional coefficient μ, and (D) decreases with increasing helix pitch λ.

Figure 6

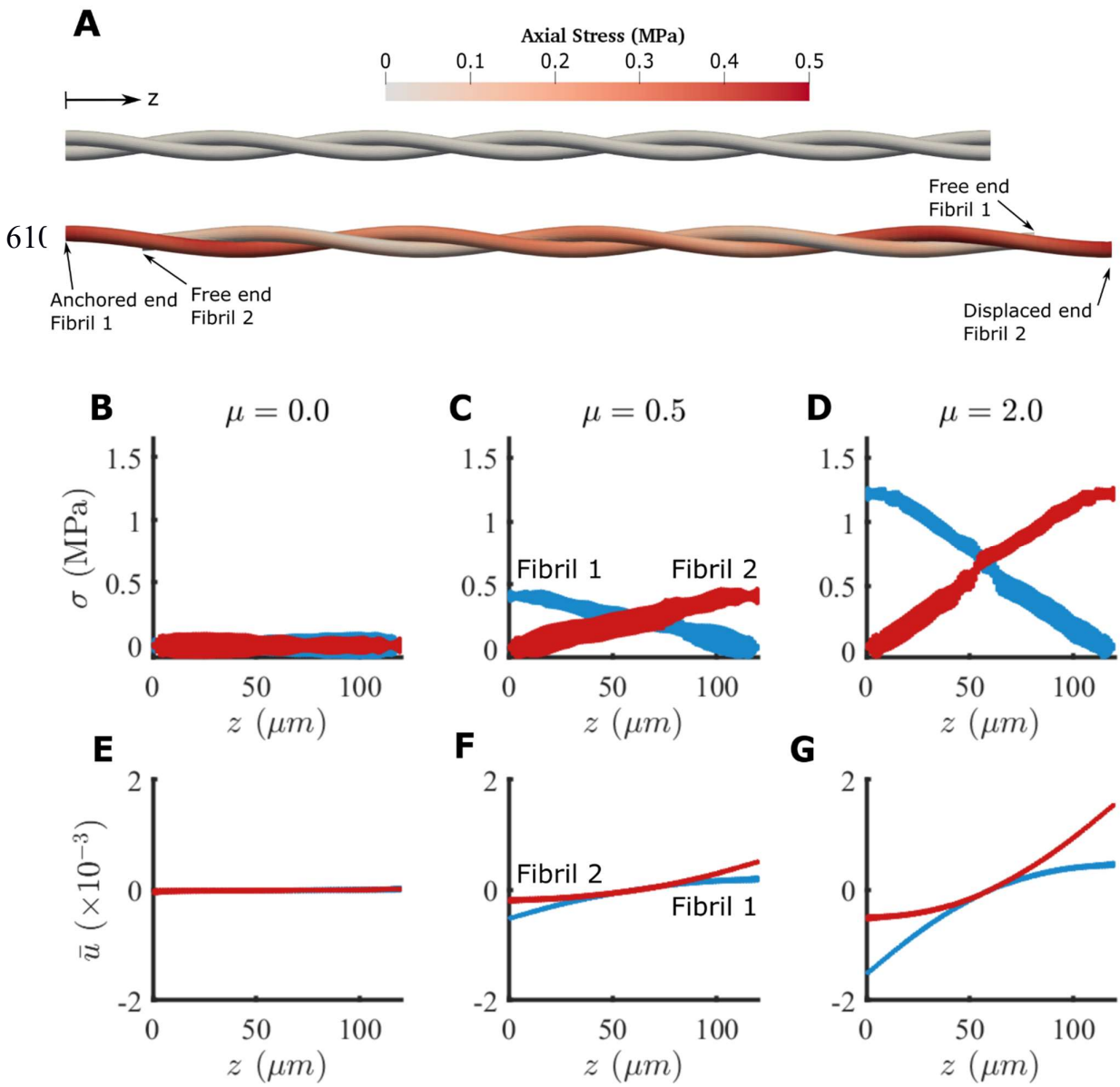

Figure 6: Finite element simulation of two helically wrapped fibrils. (A) Axial stress distribution in the fibrils for the undeformed (top) and deformed (bottom) states for $\mu = 0.5$. The geometrical scale is compacted 10 times in the axial direction for clarity. (B–D) Stress along the length of the fibrils, and (E–G) normalized displacement ($\overline{u}$, Eq. 4) along the length of the fibrils for various choices of friction coefficient μ. With no friction ($\mu = 0$) there was no σ or $\overline{u}$ (B, E). As the frictional coefficient increases, the stress and the deformation increases for $\mu = 0.5$ (C, F) and for $\mu = 2$ (D,G). The model parameters are $E = 1$ GPa, $\nu = 0.2$, $\lambda = 40\ \mu m$.